ACS APPLIED MATERIALS & INTERFACES

Research Article

www.acsami.org

Real-Time Visualizing and Tracing of HSV-TK/GCV Suicide Gene Therapy by Near-Infrared Fluorescent Quantum Dots

Dan Shao,[†,§] Jing Li,[†,§] Xuanang Xiao,[†] Ming Zhang,[†] Yue Pan,[†] Shuo Li,[‡] Zheng Wang,[†] Xin Zhang,[†] Huilin Zheng,[†] Xuewen Zhang,*[,‡] and Li Chen*[,†]

[†]Department of Pharmacology, Nanomedicine Engineering Laboratory of Jilin Province, College of Basic Medical Sciences, Jilin University, Changchun 130021, China

[‡]Department of Hepatobiliary and Pancreas Surgery, China-Japan Union Hospital of Jilin University, Changchun 130021, China

Supporting Information

ABSTRACT: Exploring intracellular behavior of suicide gene is significant for improving the efficacy and safety of herpes simplex virus thymidine kinase gene/ganciclovir (HSV-TK/GCV) system in cancer therapy. Molecular imaging represents a powerful tool to understand gene transportation and function dynamics. In this work, we reported a quantum-dot-based technique for revealing the procedure of HSV-TK/GCV suicide gene therapy by constructing covalent linkage between near-infrared fluorescent quantum dots (QDs) and TK gene. This stable QD labeling did not influence either the QDs fluorescence or the biological activity of TK gene. Furthermore, we visualized and dynamically traced the intracellular behavior antitumor effect of TK gene in vitro and in vivo. It is demonstrated that TK gene was shuttled to the nucleus after a-24 h treatment; at that time the single dose of GCV administration exerts the gradually increasing lethal effect until to 72 h. Real-time tracing the formation of hepatocellular carcinoma treated with HSV-TK/GCV suicide gene system in vivo by QD-based NIR fluorescence imaging provides useful insight toward QD-based theranostics in future cancer therapy.

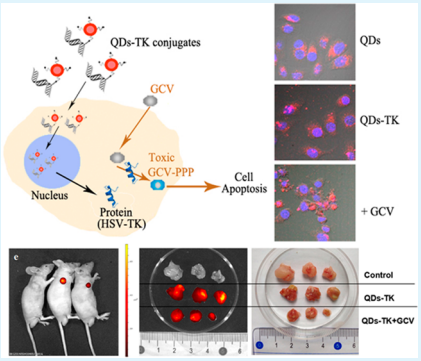

KEYWORDS: *quantum dots, HSV-TK suicide gene therapy, molecular imaging, real-time, GCV*

1. INTRODUCTION

Gene therapy appears to be a promising strategy for cancer treatment, which is evidenced by a large number of recently reported studies in vitro and in vivo.[1−3] Among various cancer gene therapy approaches, suicide gene therapy seems to be an effective system characteristic with the unique bystander effects.[4,5] Herpes simplex virus thymidine kinase gene (HSV-TK) with ganciclovir (GCV) as a predrug is extensively studied. The expression of the HSV-TK gene in tumor cells by TK transfection leads to the production of viral thymidine kinase that metabolizes GCV to ganciclovir monophosphate. Cellular kinases then convert monophosphorylated GCV into ganciclovir triphosphate, which inhibits DNA polymerase and/or incorporates into DNA, finally resulting in DNA chain termination and tumoral cell death.[6,7] The encouraging results achieved in the preclinical studies with the HSV-TK/GCV system lead to its application in several clinical trials toward different types of cancer.[8−10] However, the drawback of HSV-TK/GCV system is that TK/GCV system itself may cause normal organ damage due to TK gene entering into normal cells and toxic GCV triphosphate acumulation along with long-term administration of GCV. Therefore, we assume that GCV administration was directed by tracing dynamic behavior of TK gene, which would solve the side effect of GCV and enhance the efficacy of current HSV-TK/GCV suicide in cancer gene therapy.

Conventionally, visualizing and tracking of plasmid DNA depends on using organic fluorophores. Attempts to tag plasmid DNA with organic fluorophores have involved cumbersome procedures and the possibility of irreversible changes to the DNA with consequent loss of functional activity.[11,12] Moreover, such organic fluorophores are not ideal labels because they rapidly undergo photobleaching, which renders them unsuitable for long-term imaging studies.[13] To circumvent these problems, an ideal probe for imaging the intracellular trafficking of DNA should be developed and possess the following features, such as compatibility with cellular substrates, high stability, and capacity to emit a high-intensity signal upon illumination over long periods of time. To solve these issues, we have developed a novel procedure for labeling plasmid DNA using quantum dots. As a new category of biological labels, quantum dots (QDs) are nanometer-sized semiconducting crystals with distinct fluorescent properties, which include tunable emission from visible to infrared wavelengths by changing the size and composition, broad

Received: December 31, 2013
Accepted: June 27, 2014
Published: June 27, 2014

excitation spectra, intense brightness, photostability, and high resistance to photobleaching as compared to organic fluorophores.[14−16] With these unique features, QDs are becoming a suitable tool for both in vitro and in vivo imaging.[17−20] Recently, they have also been found to be potentially useful in visually tracking biomolecules inside living cells to elucidate some biological processes at the cellular level.[21−25] Some studies further aim to assess the recent trends and advancements made in the area of QD-based theranostic technology with an emphasis on nucleic acid biofunctionalization and delivery.[26−30] To use QDs as a tool for biological visualization in vivo, various attempts were performed to modify QDs into biocompatible fluorescent detectors and(or) immobilized QDs on biomolecules by conjugation utilizing electrostatic attraction, covalent attachment, or thiol-exchange reaction.[31−33]

Our previous studies indicated that CdTe/CdS core/shell QDs could label HSV-TK suicide gene and monitor its efficacy during a-96 h treatment in vitro,[34] but the real-time intracellular tracing TK gene as well as the optimal time of GCV administration are still unrevealed. In the present study, real-time visualizing and tracing of HSV-TK/GCV suicide gene by near-infrared fluorescent quantum dots was carried out by using the novel QDs−TK conjugates. After fabrication and characterization of QDs−TK conjugates, the intracellular localization of QDs−TK conjugates was visually tracked by confocal fluorescence microscope in different time intervals. Moreover, the optimal administration time of GCV and the therapeutic efficacy of QDs−TK conjugates were successfully investigated by MTT assay and apoptosis determination. Importantly, we real-time visualized the HSV-TK/GCV suicide gene therapy intracellular trafficking process in vitro and monitored therapeutic efficacy in vivo, which developed QD-based theranostics as a new approach to enhance the efficacy and safety of suicide gene therapy.

2. EXPERIMENTAL SECTION

2.1. Materials. Carboxyl-functionalized quantum dots (QDot 800) with emission wavelength of 800 nm were supplied by Invitrogen Corp. Institute (Carlsbad, CA, Q21371MP, 8 μM solution). QDs have a core of CdSeTe and a shell of ZnS. 1-Ethyl-3-(3-(dimethylamino)-propyl) carbodiimide hydrochloride (EDC, purity 99%), sulfo-*N*-hydroxysulfosuccunimide (sulfo-NHS, purity 98.5%), ethidium bromide (EB), and agarose gel were purchased from Sigma-Aldrich. RPMI-1640 medium and 3-(4,5-dimethylthiazol-2-yl)-2,5-diphenyl tetrazolium bromide (MTT) were obtained from GIBCO. FuGENE HD transfection reagents were purchased from Roche Applied Science. Deionized water was purified through a Milli-Q water purification system, and the resistivity was 18.2 MΩ cm. The pCMV-TK encoding the HSV-TK gene under the control of CMV promoter was kindly presented by Dr.You-Sub Won (Department of Molecular Biology, Institute of Nanosensor and Biotechnology, Dankook University).

2.2. Preparation of QDs−TK Conjugates. QDs−TK conjugates were synthesized and purificated according to the method reported previously.[34] The plasmid TK was conjugated to carboxyl-functionalized Qdot 800 classically by using EDC and sulfo-NHS (S-NHS) as cross-linking reagent. For the preparation of QDs−TK, 100 μL of QDs (8 μM) was mixed with 10 μL of EDC and sulfo-NHS successively in phosphate buffer saline (PBS, pH 7.4) with the molar ratio of 1:100:200. After 30 min of magnetic stirring, 400 μL of TE buffer (30 mM Tris-HCl, 1 mM EDTA, pH 8.0) solution consisting of equivalent molar plasmid TK (2 μM) was added into the reacted bottle and stirred at room temperature for another 3 h. To remove the excess small molecules, for example, EDC and sulfo-NHS, the resulting samples were centrifuged in Microcon Centrifugal Filter Devices (50 000 nominal molecule weight limit), and then the QDs−TK conjugates were redissolved in PBS buffer. At last, the concentrations of QDs and plasmid TK in QDs−TK conjugates were determined by a UV-2550 spectrophotometer (Shimadzu, China) and a Nano-200 Nucleic Acid Analyzer (Allsheng, China), respectively.

2.3. Characterization of QDs−TK Conjugates. UV−vis absorbance and fluorescence measurements were measured at room temperature by a UV-3101 spectrophotometer and a Hitachi F-4500 fluorescence spectrofluorimeter, respectively. Particle size distribution and zeta potential were measured by a Nano-ZS 90 Nanosizer (Malvern Instruments Ltd., Worcestershire,UK) according to the manufacturer's instructions. Fourier-transform infrared (FTIR) spectroscopy was performed on a Bruker model VECTOR22 Fourier-transform spectrometer using KBr pressed disks. Moreover, gel imaging was carried out with a Bio-Rad imaging system, the final QDs−TK conjugates were characterized by the agarose gel (0.8% w/v) electrophoresis technique, and agarose gel electrophoresis was run at 120 V/cm for 20 min.

2.4. Cell Culture and MTT Assay. Human hepatocelluar carcinoma cell lines (HepG2) were maintained at 37 °C under 5% CO_2 in RPMI-1640 (GIBCO) supplemented with 10% (v/v) heat-inactivated fetal bovine serum (FBS, Invitrogen), penicillin (100 U/mL), and streptomycin (100 μg/mL). HepG2 cells were seeded into 96-well plates at a density of 2×10^4 cells/well overnight, and then treated with QD (5−40 nM) or QDs−TK conjugates (20 nM) for different time intervals. Twenty microliters of stock MTT (5 mg/mL) was added to each well in 96-well plates, and cells were then incubated for 4 h at 37 °C. The dark blue formazan crystals formed were dissolved with DMSO. The optical density (OD) value of each well was read by a microplate reader (Sanyo Co.) at 570 nm. The survival rate of cells was expressed as A/B 100%, where A was the absorbance value from the experimental cells and B was that from the control cells.

2.5. TK Gene Transfection. The transfection procedure was performed using FuGENE HD (Roche) according to the manufacturer's instructions. Briefly, HepG2 cells were plated 24 h before transfection at a density of 1×10^6 cells per 35 mm well in antibiotic- and serum-free medium. FuGENE HD transfection reagent (5 μL) and the QDs−TK conjugates (20 μL, C_{QDs} = 1 μM) were diluted in opti-1640 (300 μL) and incubated at room temperature for 15 min. The complexes then were added to cell cultures in fresh antibiotic- and serum-free medium to the final volume of 1000 μL for transfection (the final C_{QDs} = 20 nM). The medium was replaced with serum-containing medium 6 h after transfection.

2.6. TK Protein Expression by Western Blot. After being transfected with QDs−TK conjugates for 24, 48, and 72 h, HepG2 cells were lysed with RIPA Cell Lysis Buffer (Cell Signaling) containing a protease inhibitor cocktail (Sigma) by incubating on ice for 30 min. Total protein was quantified, mixed with sample buffer, and boiled at 90 °C for 5 min. Equal amount of protein (30 mg) was separated by electrophoresis in 12% SDS-PAGE, transferred to PVDF membranes. The primary antibodies used included goat anti-TK antibody (cat. no. sc-28038, Santa Cruz Biotechnologies) prediluted 1:500, or rabbit anti-GAPDH antibody (cat. no. sc-25778, Santa Cruz Biotechnologies) prediluted 1:500. The secondary antibodies used were HRP-conjugated antigoat IgG (Invitrogen) and antirabbit IgG, both prediluted 1:5000. Protein was visualized with enhanced chemiluminescence solution, and images were generated with GENE Imaging system. The images were quantified using Image Analysis Software (Quantity One).

2.7. Determination of Apoptosis by Annexin V/PI Staining Analysis. Apoptosis was measured using an Annexin V-FITC Apoptosis Analysis Kit (Tianjin Sungene Biotech Co., Ltd., China). HepG2 cells were transfected with QDs−TK (the final C_{QDs} = 20 nM) for 6 h, GCV was added to the medium 24 h after the transfection, and then cells were harvested by trypsinization at 48, 72, and 96 h after the transfection, washed with ice-cold PBS, and suspended in binding buffer at a density of 1×10^6 cells/mL. Next, the cell suspension was stained with 5 μL of Annexin V and PI and analyzed by flow cytometry (Becton−Dickinson Biosciences, Drive Franklin Lakes, U.S.).

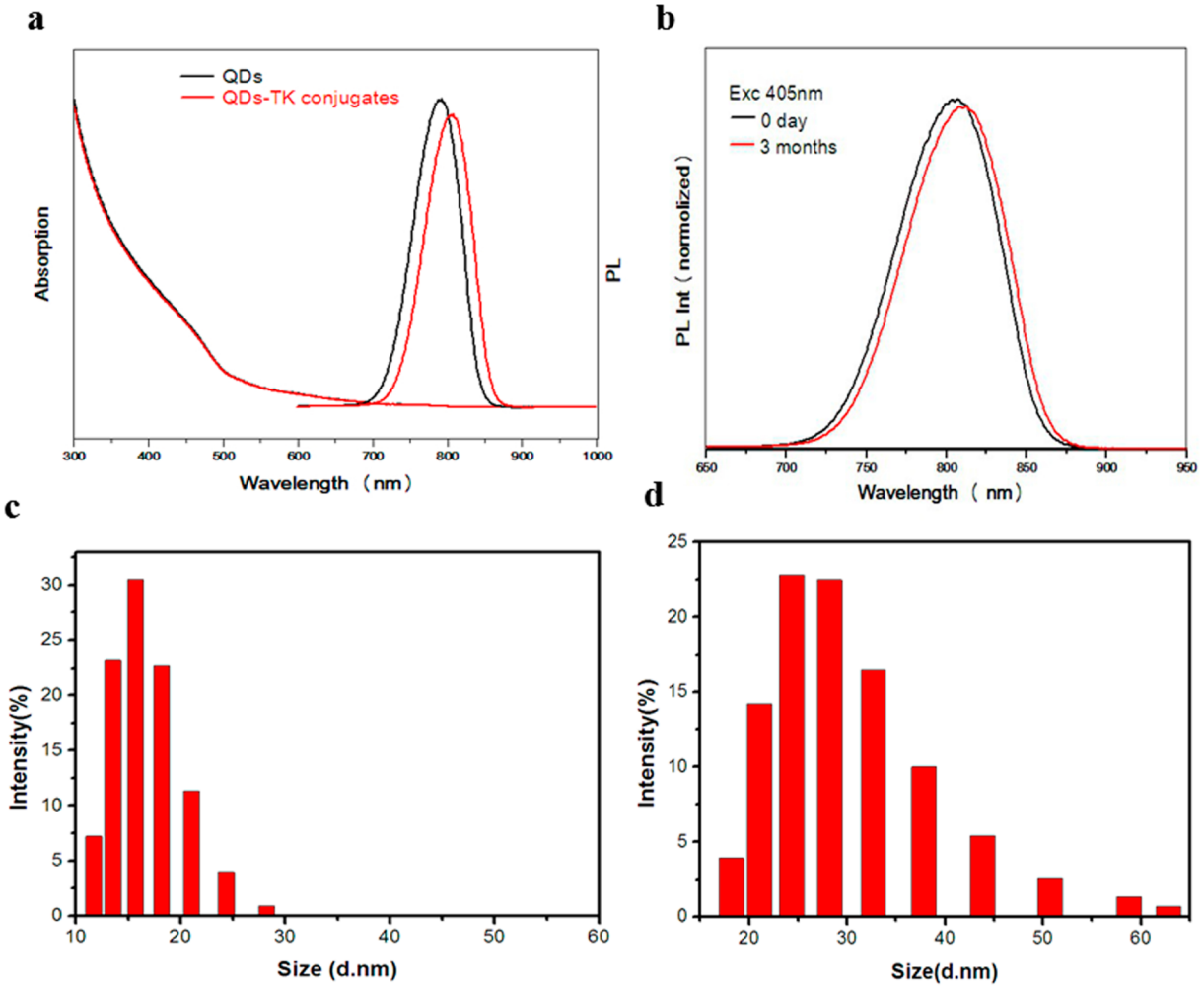

Figure 1. Characterization of QDs−TK conjugates. (a) Absorption and PL spectrum of QDs and QDs−TK conjugates. (b) The photostability of QDs−TK conjugates. The emission measurements of QDs−TK conjugates were performed at 0 day (as-synthesized) and after 3 months of storage in the dark at 4 °C. (c,d) Hydrodynamic diameter distribution of QDs and QDs−TK conjugates in water.

2.8. Confocal Microscope. After transfection in different time points, the cells were washed twice with chilled PBS, and the nuclei were stained with Hoechst 33258 (5 μg/mL) for 5 min. The cells then were rinsed again with chilled PBS. The plasmid TK intracellular location and cytotoxicity were observed by confocal laser scanning microscopy. The confocal laser scanning microscopy was carried out using a Olympus FV1000 microscope equipped with a multiline argon laser, 405, 488 nm, and 30 mW laser class 3D laser. For *z*-stack images, depths of 10 μm were captured with images taken every 1 μm.

2.9. In Vivo Real-Time Imaging of Tumor Formation. All animal experiment protocols were approved by the Ethics Committee for the Use of Experimental Animals of Jilin University. First, HepG2 cells were transfected with QDs−TK conjugates (the final C_{QDs} = 20 nM) for 6 h, then cells (2×10^6) were collected in 70 μL of PBS and mixed with 70 μL of Matrigel Matrix (Becton Dickinson Biosciences). The mixture was injected subcutaneously to one side of the flank of 6−8-week-old male BALB/c nu/nu mice (Vital River Laboratories, Beijing, China), and then the mice were divided into two groups, including QDs−TK group and QDs−TK plus GCV group for 3 mice in each group. Another 3 mice injected HepG2 cells without transfecting QDs−TK were established as the control group. The predrug GCV (50 mg/kg) was initiated by intraperitoneal injection every 3 days after the first inoculation of QDs−TK conjugates transfected cells. For real-time NIR imaging, the mice were anesthetized and imaged at designed intervals (3, 5, 7, and 14 d) after the tumor formation, and in vivo NIR images were obtained with a Xenogen IVIS Spectrum system using Living Imaging software (Caliper, Xenogen, Alameda, CA, excitation, 640 nm, emission, 760 nm long pass). All image analysis and NIR fluorescent signal quantifications were performed using the ROI function of Living Image software version 3.0 (Caliper Life Sciences). The mice were sacrificed at the 14th day after tumor formation, and all tumors are removed and weighted (n = 3 for each group). The NIR images of dissected tumor were also acquired.

2.10. Statistical Analysis. Data were expressed as mean ± SD. The statistical significance of the data was compared by Student's t test. Analysis of variance (ANOVA) was used to analyze the differences among the different groups.

3. RESULTS AND DISCUSSION

QDs−TK conjugates were synthesized and purified as reported in our previous work.[35] Briefly, plasmid TK was covalently conjugated with the carboxylate group on the surface of near-infrared fluorescent CdSeTe/ZnS core/shell QDs (Invitrogen) by EDC/sulfo-NHS-mediated amidation reaction. Next, the photoluminescence and absorption properties of QDs−TK conjugates were characterized by spectrophotometer. As shown in Figure 1a, near-infrared QDs exhibited a broad absorption cross-section, and a sharp and symmetrical band gap emission at near-infrared region. QDs−TK conjugates have slight fluorescence reduction after conjugating with TK gene, but they are still stable, even after being stored at 4 °C for 3 months

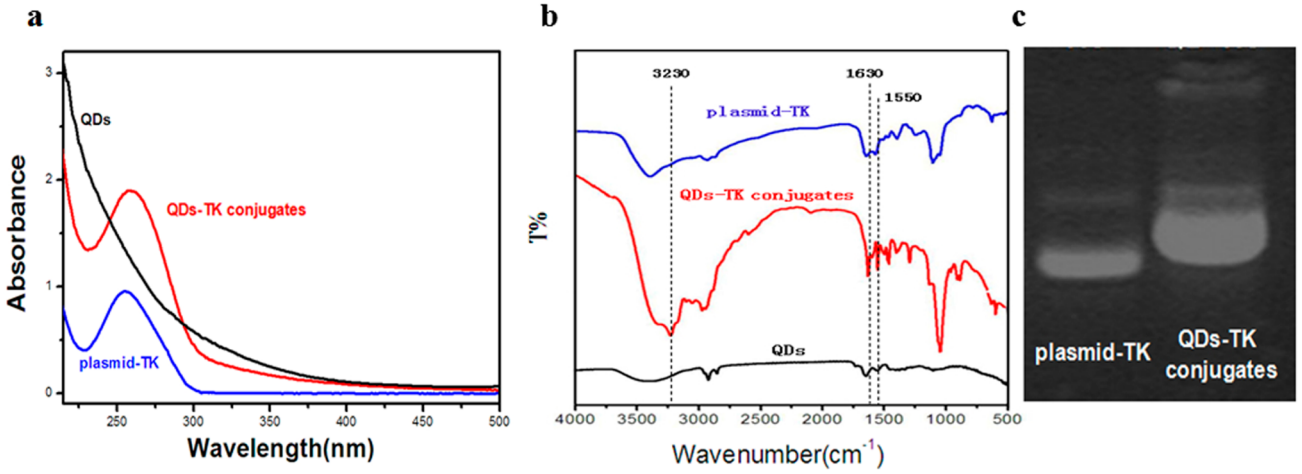

Figure 2. Confirmation of QDs−TK conjugates. (a) UV−vis absorption spectra of QDs, plasmid TK, and QDs−TK conjugates. (b) FTIR spectra of QDs and QDs−TK conjugates. (c) The agarose electrophoresis of plasmid TK and QDs−TK conjugates dyed with EB.

(shown in Figure 1b). The QD size we used in our experiment is about 16 nm (Figure 1c). After coupling with TK plasmid, the average hydrodynamic diameter is 33 nm (Figure 1d). When QDs−TK was stored at 4 °C for 3 months, the average diameter is 35 nm (Supporting Information Figure S1), which suggests QDs−TK has good storage stability. These results were consistent with transmission electron microscopy (TEM) images (shown in Supporting Information Figure S2). These data showed that QDs−TK conjugates exhibited good photo stability and storage stability. Moreover, UV−vis fluorescence, FTIR spectroscopy, and gel electrophoresis were used to confirm the conjugation of plasmid TK and QDs. After plasmid TK was conjugated to QDs, an obvious absorption peak occurs at 260 nm, as shown in Figure 2a, which is a characteristic peak of the DNA strand, indicating the successful binding between plasmid TK and QDs. FTIR was used to further confirm the conjugation of plasmid TK and QDs. In Figure 2b, the peaks at 1650 and 3400 cm^{-1} correspond to the stretching vibrations of C═O and −OH, respectively, which demonstrate the carboxylic group capping on QDs. As compared to QDs, the characteristic peaks of amide−carbonyl (NH−CO) were observed at 1630 cm^{-1} (C═O stretch), 3230 cm^{-1} (−N−H stretch), and 1550 cm^{-1} (−N−H bend) after the formation of QDs−TK conjugates, which further proves the successful connection. Furthermore, the zeta potential of QDs, plasmid TK, and QDs−TK conjugates are relatively −39.0, −12.5, and −47.6 mV, which confirmed more negative zeta potential after the conjugation. Finally, 0.8% agarose gel electrophoresis was employed to confirm QDs−TK conjugation. As shown in Figure 2c, the band of plasmid TK was ahead of QDs−TK conjugates, because the molecular weight of the QDs−TK conjugates is larger than that of plasmid TK. All of these results demonstrated the successful coupling between the QDs and plasmid TK.

To determine the safe dose of QDs as a tool for tracking suicide gene, MTT assay was conducted to evaluate cell viability on human hepatocellular carcinoma HepG2 cells treated with QDs alone. As shown in Figure 3a, the results showed the cell viability cocultured with QDs was decreased with QDs concentration increment at 96 h. When the concentration was exceeded to 40 nM, cell viability was lowered to 90%. So we prepared QDs−TK conjugates with the final concentration of 20 nM QDs, and the cytotoxicity of

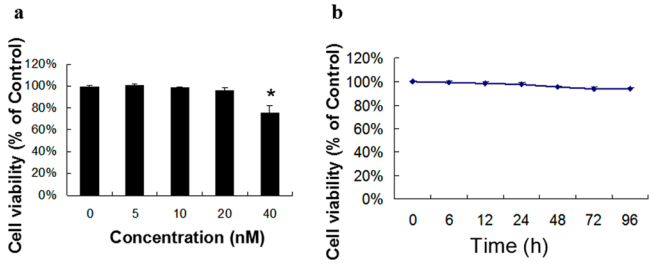

Figure 3. Safety evaluation of QDs−TK conjugates. (a) Cell viability of HepG2 cells with a-96 h treatment of different concentration QDs. (b) Cell viability of HepG2 cells treated with QDs−TK conjugates at different time points. The viability of the control cells was considered as 100%. The results are means ± SE from three independent experiments. *$P < 0.05$, versus control group.

QDs−TK conjugates was also determined at different time points (after transfecting for 6, 12, 24, 48, 72, and 96 h). As shown in Figure 3b, the results indicate that the QDs−TK conjugates have no cytotoxicity on HepG2 cells for a-96 h treatment.

To elucidate the process of TK gene trafficking in the cells and how TK gene exerts biological function, the intracellular localization of QDs−TK conjugates was monitored in HepG2 cells from 6 to 48 h under confocal fluorescence microscope. As shown in Figure 4a, QDs−TK conjugates were mainly localized in the cytoplasm, less in perinucleus within 6 h. QDs−TK conjugates started to appear in nucleus at 12 h (Figure 4b), and some QDs−TK conjugates accumulated in the nuclei at 24 h (Figure 4c) and 48 h (Figure 4d). These results indicate that QDs dynamically trace the biological behavior of TK gene in live cells, as reflected by their transportation from cytoplasm to nucleus. To further discover whether QDs−TK conjugates were indeed internalized to nucleus, but not attached on the surface of cell nucleus, *z*-stack images were taken each 1 μm apart close to the nucleus stained by Hoechst 33258. As shown in Figure 5a and b, the QDs fluorescence mainly appeared in cytoplasma around the nucleus in HepG2 cells after a-6 h transfection of QDs−TK conjugates. In contrast, the higher level of overlaying pink fluorescence was observed in 2−6 μm serial slices (*z*-stacks), demonstrating the localization of TK gene to the nucleus at a-24 h transfection, rather than the surface of nucleus. Because TK plasmid in the nucleus does not

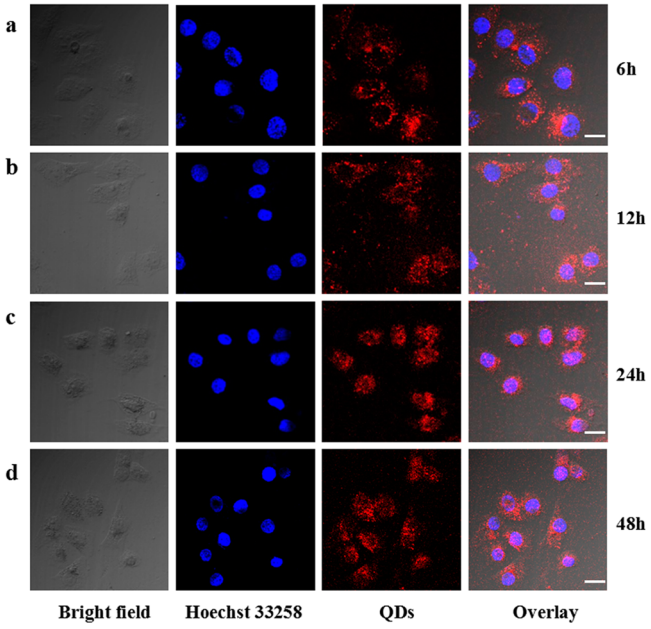

Figure 4. Real-time tracking transportation of TK gene. Confocal microscopic images were taken after cells transfected with QDs−TK conjugates at 6 h (a), 12 h (b), 24 h (c), and 48 h (d). Nucleus in HepG2 cells was stained by the Hoechst 33258, followed by washing to remove unbound materials. The QDs fluorescence signal was superimposed over the bright-field image and blue nuclear stain to show localization of TK gene. The scale bar indicates 10 μm.

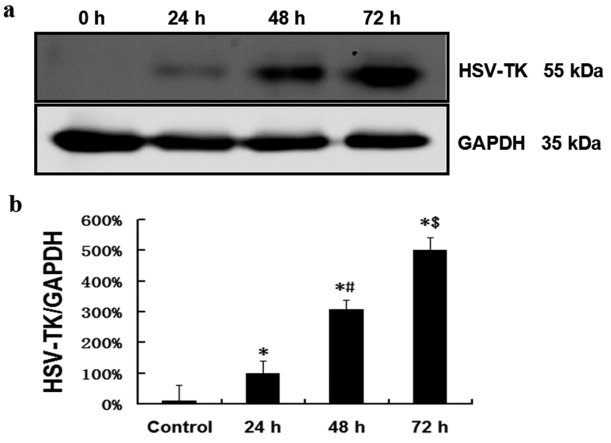

Figure 6. Protein expression of TK gene. (a) Western blot analysis showed stability of expression of HSV-TK (55 kDa) in HepG2 cells transfected with QDs−TK conjugates at 24, 48, and 72 h. GAPDH (35 kDa) was used as loading control. (b) Expression and relative quantification of protein levels expressed relative to the control. Values are the means ± SD (n = 3). $^{*}P < 0.05$ versus control group, $^{\#}P < 0.05$ versus 24 h group, $^{\$}P < 0.05$ versus 48 h group.

necessarily guarantee its translation, the corresponding relation of TK imaging and TK gene protein expression was investigated; we analyzed the protein expressions of HSV-TK at 24, 48, or 72 h after QDs−TK conjugates transfection by Western blot analysis (Figure 6). As expected, TK gene was expressed in a time-dependent manner with the initial expression occurring at 24 h, while the relative higher levels of TK expression occurred at 48 and 72 h. The results suggested that the nucleus localization of plasmid TK to some extent correlated with TK gene expression.

The efficacy of HSV-TK/GCV gene therapy depended on the expression abundance of the TK gene, as well as the available GCV in target cells.[35,36] To reveal the relationship between cellular distribution of TK gene and the efficacy of HSV-TK/GCV gene therapy, first, cell viability and apoptotic rate were evaluated by MTT assay and flow cytometry. QDs−TK conjugates combined GCV showed a time-dependent pattern on cell viability (Figure 7c) and apoptosis rate (Figure 7a and b), and the cell killing effect of the HSV-TK/GCV system after single GCV administration could be extended to 72 h. Second, the intracellular distributions in HepG2 cells treated with the QDs, QDs−TK conjugates, and QDs−TK conjugates with GCV were observed by the confocal fluorescent image. As shown in Figure 8, the fluorescent QDs distributed mostly in the cytoplasm, and the cell morphology did not change in QDs alone group. However, HepG2 cells transfected with QDs−TK conjugates in the presence of GCV showed cell shrinkage and deformation with chromatin aggregation, while cells transfected with QDs−TK presented normal morphology in the absence of GCV. Interestingly, the damaged cells have stronger fluorescent intensity than normal cells (Figure 8c); these results show that QDs could not only track and identify the intracellular localization of plasmid TK through time, but also monitor the efficacy of the HSV-TK/GCV system.

Because NIR quantum dots-labeled HSV-TK/GCV suicide gene therapy was efficient in HepG2 cells in vitro, we next examined its efficacy in vivo using subcutaneous tumor model in BALB/c nu/nu mice. Nine mice were divided into three groups, including control group, QDs−TK group, and QDs−TK plus GCV group. Real-time optical imaging was done on days 3, 5, 7, and 14. As shown in Figure 9, the average fluorescence signal in QDs−TK plus GCV group was similar in day 3 and slightly lower on day 5, and drastically dropped by day 14 as compared to QDs−TK group, which reflected to the process of tumor regression. It indicated that NIR quantum dots could real-time monitor the tumor formation with the

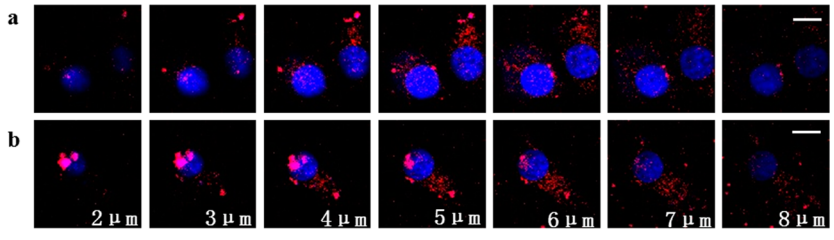

Figure 5. Confirmation of the intracellular location of TK gene. z-Stack images were taken from HepG2 cells transfected with QDs−TK conjugates for 6 h (a) or 24 h (b) at various focal depths from 2 to 8 μm. The pink dots indicated the colocalization of red QDs with the blue nuclear stain (Hoechst 33258). The scale bar indicates 10 μm.

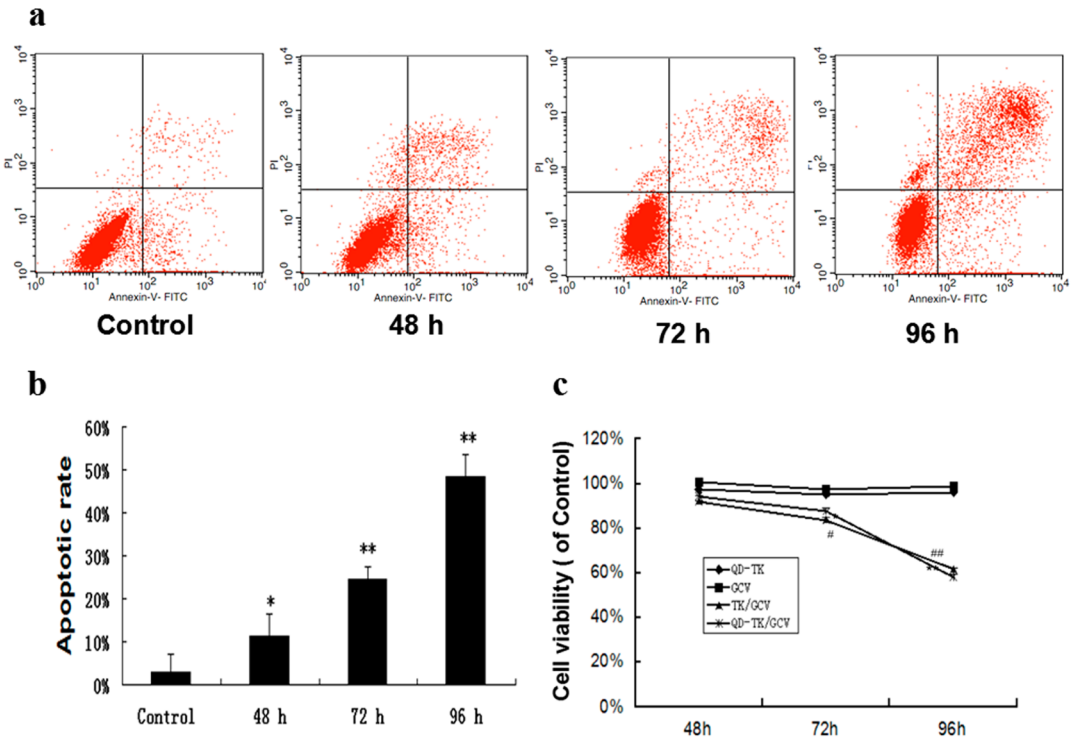

Figure 7. Evaluation of cell killing efficiency of QDs−TK/GCV. (a) The apoptosis assay on HepG2 cells after treatment of GCV for 24, 48, and 72 h (equivalent to after transfection 48, 72, and 96 h) by annexin V-FITC/PI double staining. (b) The proportion of apoptotic cells after the QDs−TK/GCV treatment. The results are means ± SD from three independent experiments.*$P < 0.05$, **$P < 0.01$, TK/GCV group versus control group, the cells in control group are treated neither by QDs−TK nor by GCV. (c) MTT assay used to determine the effect of QDs−TK conjugates on cell viability after the treatment of GCV for 24, 48, and 72 h (equivalent to after transfection 48, 72, and 96 h). The results are means ± SD from three independent experiments.*$P < 0.05$, **$P < 0.01$, QDs−TK/GCV group versus control group. $^{\#}P < 0.05$, $^{\#\#}P < 0.01$, TK/GCV group versus control group.

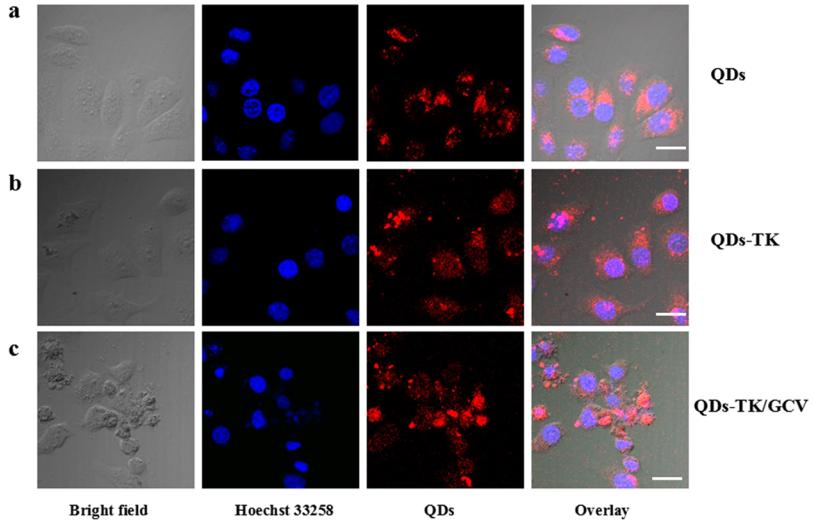

Figure 8. Monitoring antitumoral activity of QDs−TK conjugates. The imaging of HepG2 cells was observed under confocal microscopy after transfection for 96 h with the QDs or QDs−TK conjugates with or without GCV. Confocal micrographs of HepG2 cells were transfected QDs alone (a) or QDs−TK conjugates (b), as well as transfected QDs−TK conjugates with a-72 h GCV treatment (c). The scale bar indicates 10 μm.

treatment of HSV-TK/GCV suicide gene system. As shown in Figure 10, QDs−TK conjugates transduced tumors with GCV caused a significant reduction of tumor growth in comparison with the absence of GCV group and control group. The fluorescent intensity at the tumor site was significantly reduced for the mice treated with GCV, which is consistent with the decreased tumor weight in GCV treatment group. These results indicated that NIR quantum dots could facilitate the monitoring of HSV-TK/GCV suicide gene therapy in vivo by molecular imaging noninvasively.

In traditional GCV schedule, GCV administration is prior to the injection of TK gene in vivo experiment because the exact TK protein expression time course is unclear.[37,38] In addition, continuous GCV administration was used and resulted in the

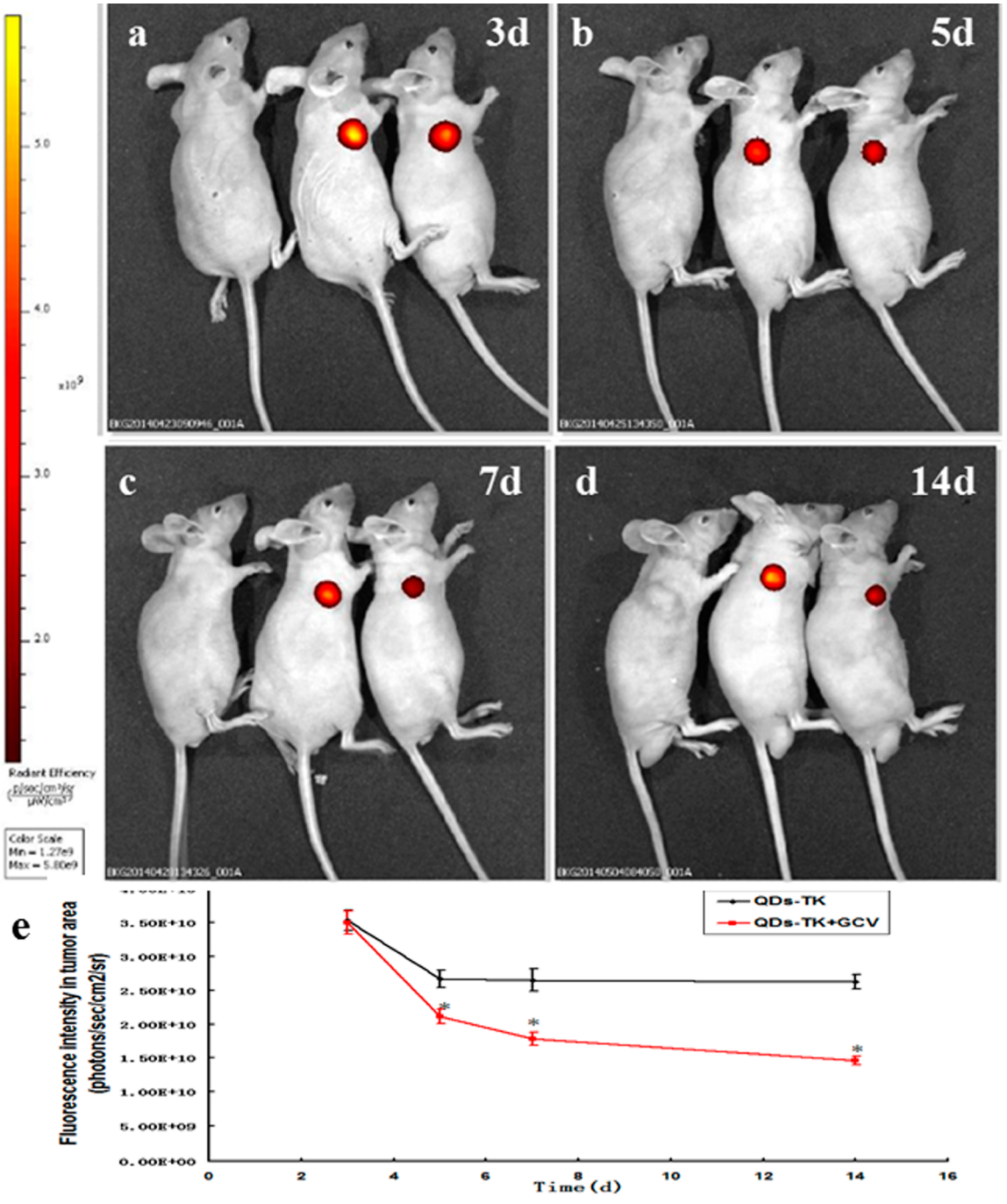

Figure 9. Real-time monitoring tumor formation. Monitoring representative images of noninvasive NIR imaging for HepG2 cells transfected with QDs−TK conjugates with or without GCV treatment throughout the imaging time points (a) 3 d, (b) 5 d, (c) 7 d, and (d) 14 d. (e) Quantitative analysis of NIR fluorescence signals of mice being shown as photons/s/cm^2/sr. Data are represented as means ± SD, n = 3, *P < 0.05 versus QDs−TK conjugates group.

acumulation of GCV causing normal organ damage. To solve this problem, our study tried another method to acquire the transportation of TK gene imaging and see if that correlated with TK protein expression and TK activity, and improve the GCV administration schedule to reduce the adverse effect of suicide gene system. We found that TK imaging revealed that the accumulation of TK gene in the nucleus was at 24 h transfection, the initial TK protein expression was also at 24 h transfection, and the higher level protein expression was gradually increasing from 48 to 72 h. Therefore, we changed the GCV administrating schedule to 24 h after transfection of QDs−TK in vitro experiment, and the administration period was every 3 days in vivo experiment. Althouth GFP and luciferase report gene were the mainstay strategy to monitor suicide gene expression,[39,40] our study wanted to try another material for real-time tracing suicide gene transportation and the efficacy. It indicated that QDs labeling represented an ideal tool for tracking plasmid TK, and simultaneously directing the optimal cycle of GCV administration to alleviate the long-term toxicity. It also sheds light on using the QDs−TK conjugates in future studies to gain a better understanding of tracking suicide gene therapy.

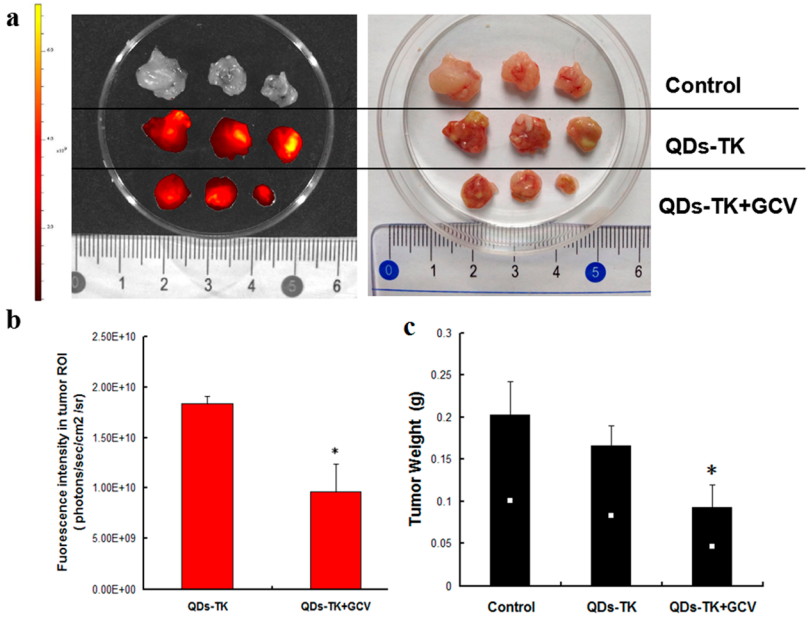

Figure 10. In vivo suicide gene therapy. (a) NIR fluorescent and white light photographs of representative xenograft tumors harvested at the end of treatment. (b) Fluorescence intensity of the excised tumors. Data are represented as means ± SD, $n = 3$, $^*P < 0.05$ versus QDs−TK conjugates group. (c) Tumor weight analysis after treatment. Data are represented as means ± SD, $n = 3$, $^*P < 0.05$ versus QDs−TK conjugates group.

4. CONCLUSIONS

In summary, we reported a QD-based labeling technique for real-time visualizing and tracing of HSV-TK/GCV suicide gene therapy by constructing covalent linkage between near-infrared fluorescent quantum dots and TK gene. This stable QD labeling did not influence either QDs fluorescence or the biological activity of TK gene. Furthermore, QDs−TK conjugates were shuttled to the nucleus after a-24 h treatment; single GCV administration at that time point exerts the gradually increasing lethal effect of the suicide gene, which provides the clue for GCV administration schedule improvement based on monitoring TK gene imaging and activity. This noninvasive imaging techniques for gene therapy monitoring will enable real-time assessment of the therapeutic process and the refinement of current treatment protocols. Our study sheds light on QD-based cancer gene therapy in future studies to improve its efficacy and safety for human application and support future individualized treatment.

■ ASSOCIATED CONTENT

Supporting Information

Further experimental details and figures, and characterization of QDs−TK conjugates. This material is available free of charge via the Internet at http://pubs.acs.org.

■ AUTHOR INFORMATION

Corresponding Authors

*E-mail: chen_lab@163.com.
*E-mail: zxw515@sohu.com.

Author Contributions

§These authors contributed equally.

Notes

The authors declare no competing financial interest.

■ ACKNOWLEDGMENTS

We thank Prof. Bai Yang, Prof. Wenfei Dong, Prof. Xianggui Kong, Prof. Qinghui Zeng, Prof. Guangfan Chi, Dr. Fangzhong Shen, Dr. Shuang Li, Dr. Yingshuai Wang, Dr. Haotong Wei, Dr. Qiongshu Li, Haiyang Wang, and Erin Lau for their help. Funding for this work is from National Natural Science Foundation of China (81071886, 81201804), the Science and Technology Support Program of Jilin Province (201205006), the Graduate Innovation Fund of Jilin University (20121118), the Opening Project of State Key Laboratory of Supramolecular Structure and Materials of Jilin University under Grant nos. SKLSSM 200912 and SKLSSM 201317, and Ph.D. Programs Foundation of Ministry of Education of China (20120061120079).

■ REFERENCES

(1) Guan, Y. S.; Liu, Y.; He, Q.; Li, X.; Yang, L.; Hu, Y.; La, Z. P53 Gene Therapy in Combination with Transcatheter Arterial Chemoembolization for HCC: One-Year Follow-Up. *World J. Gastroenterol.* **2011**, *17*, 2143−9.

(2) Sterman, D. H.; Recio, A.; Haas, A. R.; Vachani, A.; Katz, S. I.; Gillespie, C. T.; Cheng, G.; Sun, J.; Moon, E.; Pereira, L.; Wang, X.; Heitjan, D. F.; Litzky, L.; June, C. H.; Vonderheide, R. H.; Carroll, R. G.; Albelda, S. M. A Phase I Trial of Repeated Intrapleural Adenoviral-Mediated Interferon-Beta Gene Transfer for Mesothelioma and Metastatic Pleural Effusions. *Mol. Ther.* **2010**, *18*, 852−60.

(3) Ginn, S. L.; Alexander, I. E.; Edelstein, M. L.; Abedi, M. R.; Wixon, J. Gene Therapy Clinical Trials Worldwide to 2012-an Update. *J. Gene Med.* **2013**, *15*, 65−77.

(4) Duarte, S.; Carle, G.; Faneca, H.; de Lima, M. C.; Pierrefite-Carle, V. Suicide Gene Therapy in Cancer: Where Do We Stand Now? *Cancer Lett.* **2012**, *324*, 160−70.

(5) Morgan, R. A. A New Suicide Gene Therapy Moves to the Clinic. *Mol. Ther.* **2012**, *20*, 11−3.

(6) Balfour, H. H., Jr. Antiviral Drugs. *N. Engl. J. Med.* **1999**, *340*, 1255−68.

(7) Wang, J.; Lu, X. X.; Chen, D. Z.; Li, S. F.; Zhang, L. S. Herpes Simplex Virus Thymidine Kinase and Ganciclovir Suicide Gene

Therapy for Human Pancreatic Cancer. *World J. Gastroenterol.* **2004**, *10*, 400−3.
(8) Xu, F.; Li, S.; Li, X. L.; Guo, Y.; Zou, B. Y.; Xu, R.; Liao, H.; Zhao, H. Y.; Zhang, Y.; Guan, Z. Z.; Zhang, L. Phase I and Biodistribution Study of Recombinant Adenovirus Vector-Mediated Herpes Simplex Virus Thymidine Kinase Gene and Ganciclovir Administration in Patients with Head and Neck Cancer and Other Malignant Tumors. *Cancer Gene Ther.* **2009**, *16*, 723−30.
(9) Rainov, N. G. A Phase Iii Clinical Evaluation of Herpes Simplex Virus Type 1 Thymidine Kinase and Ganciclovir Gene Therapy as an Adjuvant to Surgical Resection and Radiation in Adults with Previously Untreated Glioblastoma Multiforme. *Cancer Gene Ther.* **2000**, *11*, 2389−401.
(10) Nasu, Y.; Saika, T.; Ebara, S.; Kusaka, N.; Kaku, H.; Abarzua, F.; Manabe, D.; Thompson, T. C.; Kumon, H. Suicide Gene Therapy with Adenoviral Delivery of HSV-TK Gene for Patients with Local Recurrence of Prostate Cancer after Hormonal Therapy. *Mol. Ther.* **2007**, *15*, 834−40.
(11) Tanimoto, M.; Kamiya, H.; Minakawa, N.; Matsuda, A.; Harashima, H. No Enhancement of Nuclear Entry by Direct Conjugation of a Nuclear Localization Signal Peptide to Linearized DNA. *Bioconjugate Chem.* **2003**, *14*, 1197−202.
(12) Kizzire, K.; Khargharia, S.; Rice, K. G. High-Affinity Pegylated Polyacridine Peptide Polyplexes Mediate Potent in Vivo Gene Expression. *Gene Ther.* **2013**, *20*, 407−16.
(13) Ozawa, T.; Yoshimura, H.; Kim, S. B. Advances in Fluorescence and Bioluminescence Imaging. *Anal. Chem.* **2013**, *85*, 590−609.
(14) Leutwyler, W. K.; Bürgi, S. L.; Burgl, H. Semiconductor Clusters, Nanocrystals, and Quantum Dots. *Science* **1996**, *271*, 933.
(15) Klimov, V. I.; Mikhailovsky, A. A.; Xu, S.; Malko, A.; Hollingsworth, J. A.; Leatherdale, C. A.; Eisler, H.; Bawendi, M. G. Optical Gain and Stimulated Emission in Nanocrystal Quantum Dots. *Science* **2000**, *290*, 314−7.
(16) Lodahl, P.; Floris Van Driel, A.; Nikolaev, I. S.; Irman, A.; Overgaag, K.; Vanmaekelbergh, D.; Vos, W. L. Controlling the Dynamics of Spontaneous Emission from Quantum Dots by Photonic Crystals. *Nature* **2004**, *430*, 654−7.
(17) Medintz, I. L.; Uyeda, H. T.; Goldman, E. R.; Mattoussi, H. Quantum Dot Bioconjugates for Imaging, Labelling and Sensing. *Nat. Mater.* **2005**, *4*, 435−46.
(18) Michalet, X.; Pinaud, F. F.; Bentolila, L. A.; Tsay, J. M.; Doose, S.; Li, J. J.; Sundaresan, G.; Wu, A. M.; Gambhir, S. S.; Weiss, S. Quantum Dots for Live Cells, in Vivo Imaging, and Diagnostics. *Science* **2005**, *307*, 538−44.
(19) Gao, X.; Cui, Y.; Levenson, R. M.; Chung, L. W.; Nie, S. In Vivo Cancer Targeting and Imaging with Semiconductor Quantum Dots. *Nat. Biotechnol.* **2004**, *22*, 969−76.
(20) Yu, K.; Ng, P.; Ouyang, J.; Zaman, M. B.; Abulrob, A.; Baral, T. N.; Fatehi, D.; Jakubek, Z. J.; Kingston, D.; Wu, X.; Liu, X.; Hebert, C.; Leek, D. M.; Whitfield, D. M. Low-Temperature Approach to Highly Emissive Copper Indium Sulfide Colloidal Nanocrystals and Their Bioimaging Applications. *ACS Appl. Mater. Interfaces* **2013**, *5*, 2870−80.
(21) Luo, K.; Li, S.; Xie, M.; Wu, D.; Wang, W.; Chen, R.; Huang, L.; Huang, T.; Pang, D.; Xiao, G. Real-Time Visualization of Prion Transport in Single Live Cells Using Quantum Dots. *Biochem. Biophys. Res. Commun.* **2010**, *394*, 493−7.
(22) Liu, S. L.; Zhang, Z. L.; Sun, E. Z.; Peng, J.; Xie, M.; Tian, Z. Q.; Lin, Y.; Pang, D. W. Visualizing the Endocytic and Exocytic Processes of Wheat Germ Agglutinin by Quantum Dot-Based Single-Particle Tracking. *Biomaterials* **2011**, *32*, 7616−24.
(23) Liu, S. L.; Zhang, Z. L.; Tian, Z. Q.; Zhao, H. S.; Liu, H.; Sun, E. Z.; Xiao, G. F.; Zhang, W.; Wang, H. Z.; Pang, D. W. Effectively and Efficiently Dissecting the Infection of Influenza Virus by Quantum-Dot-Based Single-Particle Tracking. *ACS Nano* **2012**, *6*, 141−50.
(24) Zaman, M. B.; Baral, T. N.; Zhang, J. B.; Whitfield, D.; Yu, K. Single-Domain Antibody Functionalized CdSe/ZnS Quantum Dots for Cellular Imaging of Cancer Cells. *J. Phys. Chem. C* **2009**, *113*, 496−99.
(25) Ma, G. Background-Free in Vivo Time Domain Optical Molecular Imaging Using Colloidal Quantum Dots. *ACS Appl. Mater. Interfaces* **2013**, *5*, 2835−44.
(26) Qian, J.; Gao, X. Triblock Copolymer-Encapsulated Nanoparticles with Outstanding Colloidal Stability for siRNA Delivery. *ACS Appl. Mater. Interfaces* **2013**, *5*, 2845−52.
(27) Chong, L.; Vannoy, C. H.; Noor, M. O.; Krull, U. J. Intracellular Nucleic Acid Interactions Facilitated by Quantum Dots: Conceptualizing Theranostics. *Ther. Delivery* **2012**, *3*, 479−99.
(28) Li, Y.; Duan, X.; Jing, L.; Yang, C.; Qiao, R.; Gao, M. Quantum Dot-Antisense Oligonucleotide Conjugates for Multifunctional Gene Transfection, mRNA Regulation, and Tracking of Biological Processes. *Biomaterials* **2011**, *32*, 1923−31.
(29) Zhang, P.; Liu, W. ZnO QD@PMAA-Co-PDMAEMA Nonviral Vector for Plasmid DNA Delivery and Bioimaging. *Biomaterials* **2010**, *31*, 3087−94.
(30) Li, S.; Liu, Z.; Ji, F.; Xiao, Z.; Wang, M.; Peng, Y.; Zhang, Y.; Liu, L.; Liang, Z.; Li, F. Delivery of Quantum Dot-siRNA Nanoplexes in SK-N-SH Cells for Bace1 Gene Silencing and Intracellular Imaging. *Mol. Ther.* **2012**, *1*, 20.
(31) Dubertret, B.; Skourides, P.; Norris, D. J.; Noireaux, V.; Brivanlou, A. H.; Libchaber, A. In Vivo Imaging of Quantum Dots Encapsulated in Phospholipid Micelles. *Science* **2002**, *298*, 1759−62.
(32) Zhan, N.; Palui, G.; Grise, H.; Tang, H.; Alabugin, I.; Mattoussi, H. Combining Ligand Design with Photoligation to Provide Compact, Colloidally Stable, and Easy to Conjugate Quantum Dots. *ACS Appl. Mater. Interfaces* **2013**, *5*, 2861−9.
(33) Wang, Y.; Chen, L. Quantum Dots, Lighting up the Research and Development of Nanomedicine. *Nanomedicine (N. Y., NY, U. S.)* **2011**, *7*, 385−402.
(34) Shao, D.; Zeng, Q.; Fan, Z.; Li, J.; Zhang, M.; Zhang, Y.; Li, O.; Chen, L.; Kong, X.; Zhang, H. Monitoring HSV-TK/Ganciclovir Cancer Suicide Gene Therapy Using CdTe/CdS Core/Shell Quantum Dots. *Biomaterials* **2012**, *33*, 4336−44.
(35) Moriuchi, S.; Krisky, D. M.; Marconi, P. C.; Tamura, M.; Shimizu, K.; Yoshimine, T.; Cohen, J. B.; Glorioso, J. C. HSV Vector Cytotoxicity Is Inversely Correlated with Effective TK/GCV Suicide Gene Therapy of Rat Gliosarcoma. *Gene Ther.* **2000**, *7*, 1483−90.
(36) Azatian, A.; Yu, H.; Dai, W.; Schneiders, F. I.; Botelho, N. K.; Lord, R. V. Effectiveness of HSV-TK Suicide Gene Therapy Driven by the GRP78 Stress-Inducible Promoter in Esophagogastric Junction and Gastric Adenocarcinomas. *J. Gastrointest. Surg.* **2009**, *13*, 1044−51.
(37) Wang, L.; Su, W.; Liu, Z.; Zhou, M.; Chen, S.; Chen, Y.; Lu, D.; Liu, Y.; Fan, Y.; Zheng, Y.; Han, Z.; Kong, D.; Wu, J. C.; Xiang, R.; Li, Z. CD44 Antibody-Targeted Liposomal Nanoparticles for Molecular Imaging and Therapy of Hepatocellular Carcinoma. *Biomaterials* **2012**, *33*, 5107−14.
(38) Zhang, T. Y.; Huang, B.; Yuan, Z. Y.; Hu, Y. L.; Tabata, Y.; Gao, J. Q. Gene Recombinant Bone Marrow Mesenchymal Stem Cells as a Tumor-Targeted Suicide Gene Delivery Vehicle in Pulmonary Metastasis Therapy Using Non-Viral Transfection. *Nanomedicine (N. Y., NY, U. S.)* **2014**, *10*, 257−67.
(39) Jacobs, A.; Dubrovin, M.; Hewett, J.; Sena-Esteves, M.; Tan, C. W.; Slack, M.; Sadelain, M.; Breakefield, X. O.; Tjuvajev, J. G. Functional Coexpression of HSV-1 Thymidine Kinase and Green Fluorescent Protein: Implications for Noninvasive Imaging of Transgene Expression. *Neoplasia* **1999**, *1*, 154−61.
(40) Waerzeggers, Y.; Monfared, P.; Viel, T.; Winkeler, A.; Voges, J.; Jacobs, A. H. Methods to Monitor Gene Therapy with Molecular Imaging. *Methods* **2009**, *48*, 146−60.